

Reflectance of graphene-coated dielectric plates in the framework of Dirac model: Joint action of energy gap and chemical potential

G. L. Klimchitskaya^{1,2}, V. S. Malyi², V. M. Mostepanenko^{1,2,3}
and V. M. Petrov²

¹Central Astronomical Observatory at Pulkovo of the Russian Academy of Sciences, St.Petersburg, 196140, Russia

²Institute of Physics, Nanotechnology and Telecommunications, Peter the Great Saint Petersburg Polytechnic University, St.Petersburg, 195251, Russia

³Kazan Federal University, Kazan, 420008, Russia

E-mail: vmostepa@gmail.com

Abstract. We investigate the reflectance of a dielectric plate coated with a graphene sheet which possesses the nonzero energy gap and chemical potential at any temperature. The general formalism for the reflectance using the polarization tensor is presented in the framework of Dirac model. It allows calculation of the reflectivity properties for any material plate coated with real graphene sheet on the basis of first principles of quantum electrodynamics. Numerical computations of the reflectance are performed for the graphene-coated SiO₂ plate at room, liquid-nitrogen, and liquid-helium temperatures. We demonstrate that there is a nontrivial interplay between the chemical potential, energy gap, frequency, and temperature in their joint action on the reflectance of a graphene-coated plate. Specifically, it is shown that at the fixed frequency of an incident light an increase of the chemical potential and the energy gap affect the reflectance in opposite directions by increasing and decreasing it, respectively. According to our results, the reflectance approaches unity at sufficiently low frequencies and drops to that of an uncoated plate at high frequencies for any values of the chemical potential and energy gap. The impact of temperature on the reflectance is found to be more pronounced for graphene coatings with smaller chemical potentials. The obtained results could be applied for optimization of optical detectors and other devices exploiting graphene coatings.

Keywords: graphene-coated plate, energy gap, chemical potential, reflectance

1. Introduction

Investigation of graphene, a two-dimensional sheet of carbon atoms packed in a hexagonal lattice, has clearly demonstrated unique opportunities of this material for both fundamental and applied physics. The Dirac model is of primary importance for understanding the physical properties of graphene. According to this model, at energies below one or two eV the quasiparticles in graphene are either massless or very light and obey the linear dispersion relation although move with the Fermi velocity v_F which is less than the speed of light c by approximately a factor of 300 (see [1–3]).

Theoretical description of the electrical conductivity and reflectances of graphene has been developed in the framework of the Kubo response theory, the Boltzmann transport equation, the formalism of the correlation functions in the random phase approximation and some other, more phenomenological approaches, such as the two-dimensional Drude model. This provided insight into the nature of optical properties of graphene and offered a clearer view on its universal conductivity expressed via the electric charge e and the Planck constant \hbar [4–14]. Some of the theoretical approaches mentioned above have been applied also to calculate the Casimir (Casimir-Polder) force between two graphene sheets and between an atom and graphene which is caused by the zero-point and thermal fluctuations of the electromagnetic field [15–28]. It should be mentioned, however, that the cited theoretical approaches are not based on the first principles of quantum electrodynamics at nonzero temperature which should be directly applicable to a simple system described by the Dirac model. In this connection, due to some ambiguities in the statistical description and limiting transitions, several conflicting results related to the conductivity, optical properties and Casimir forces in graphene systems have been obtained (see a discussion [29–31]).

The most fundamental description of the optical properties, Casimir effect and electrical conductivity of graphene is given by the polarization tensor in (2+1)-dimensional space-time. Although in some specific cases this quantity was considered by many authors (see, e.g., [32–34]), the exact expressions valid at any temperature for graphene with nonzero energy gap have been derived only recently [35, 36]. The application region of the obtained polarization tensor was, however, restricted to pure imaginary Matsubara frequencies. Because of this, it was possible to apply it for detailed investigation of the Casimir effect in graphene systems [31, 37–46], but not for calculations of the reflectances and conductivities of graphene which are defined at real frequencies.

The polarization tensor valid for a gapped graphene over the entire plane of complex frequencies, including the real frequency axis, was derived in [47, 48]. In [49, 50] the results of [47, 48] were generalized for the case of graphene with nonzero chemical potential. The novel form of the polarization tensor [47–50] has been used for a more detailed study of the Casimir effect in graphene systems [51–57] and for investigation of the electrical conductivity of graphene on the basis of first principles of quantum electrodynamics at nonzero temperature [58–61]. Special attention was devoted to

the field-theoretical description of the reflectivity properties of graphene. In [47, 48] and [62] they were investigated in detail for both pure (gapless) and gapped graphene, respectively, and in [63] the joint action of nonzero energy gap and chemical potential was analyzed.

Of particular interest is the configuration of a dielectric plate coated with a graphene sheet. In addition to the fundamental interest in this subject, graphene coatings find prospective technological applications to optical detectors, various optoelectronic devices, solar cells, biosensors etc. [64–67]. Using the polarization tensor of [47, 48], the reflectivity properties of material plates coated with pure [68, 69] and gapped [70] graphene have been investigated. The case of thin films coated with gapped graphene has been considered as well [71]. However, the joint action of nonzero energy gap and chemical potential on the reflectivity properties of graphene-coated plates, which is of major interest for condensed matter physics and its applications, remains to date unexplored.

In this paper, we present the formalism using the polarization tensor of [47–50] and calculate the reflectance of the dielectric plate coated with real graphene sheet which possesses nonzero energy gap in the spectrum of quasiparticles and chemical potential. Thus, here we exploit the same formalism, as was used in Refs. [51–57] in the Casimir configurations of two parallel graphene sheets (graphene-coated plates), but in quite different physical situation. All computations are performed at the room temperature $T = 300$ K, at the liquid-nitrogen temperature $T = 77$ K, and at the liquid-helium temperature $T = 4.4$ K for the plate made of silica glass SiO_2 . It is shown that there is an interesting interplay between the chemical potential, energy gap, frequency and temperature in their impact on the reflectance of a graphene-coated plate.

Another result obtained is that at the fixed frequency ω the increasing chemical potential and energy gap affect the reflectance in opposite directions. Specifically, an increase of the chemical potential either increases the reflectance or leaves it unchanged. On the other hand, an increase of the energy gap either decreases the reflectance or leaves it constant. It is shown that for any values of the chemical potential and energy gap the reflectance of a graphene-coated plate approaches unity at sufficiently low frequencies. With increasing frequency, the reflectance drops to that of an uncoated plate. According to our results, for larger chemical potential the frequency region, where the reflectance of a graphene-coated plate depends on the presence of coating, becomes wider. However, at frequencies $\hbar\omega > 20$ meV the graphene coating makes no impact on the reflectance of a SiO_2 plate any more. An impact of temperature on the reflectance is more pronounced for graphene coating with smaller chemical potentials. For sufficiently high chemical potential, temperature no longer affects the reflectance. By and large, the presented formalism allows computation of the impact of graphene coating on the reflectance of a plate made of any material.

The paper is organized as follows. In Section 2 we present the formalism of the Dirac model expressing the reflectance of a graphene-coated plate via the polarization tensor. Section 3 contains the computational results for the reflectance as a function

of frequency and chemical potential under the varying energy gap and temperature. In Section 4 the reflectance is considered as a function of energy gap under different values of the chemical potential and temperature. In Section 5 the reader will find our conclusions and a discussion.

2. General formalism for the reflectance

We consider sufficiently thick dielectric plate, which can be treated as a semispace, coated with gapped graphene possessing some chemical potential μ . It is well known that for a pure freestanding graphene the energy gap in the spectrum of quasiparticles $\Delta = 0$, but under an influence of the defects of structure, electron-electron interaction and in the presence of a material substrate the nonzero gap $\Delta \leq 0.1$ or 0.2 eV arises [1, 3, 34, 72, 73]. As to the chemical potential, it describes the doping concentration, which is nonzero for any real graphene sample and takes typical values $\mu \sim 0.1$ eV [3]. Below we consider only the case of normal incidence so that the projection of the wave vector on a graphene plane $k = 0$ (a dependence on the incident angle is discussed in [63, 68, 70]). Because of this, it is sufficient to consider only the transverse magnetic (TM), i.e., p -polarized, electromagnetic waves of frequency ω incident on a graphene-coated plate.

The TM reflection coefficient on the dielectric plate coated with a graphene sheet is given by [46]

$$r_{\text{TM}}^{(g,p)}(\omega, 0) = \frac{r_{\text{TM}}^{(g)}(\omega, 0) + r_{\text{TM}}^{(p)}(\omega, 0)[1 - 2r_{\text{TM}}^{(g)}(\omega, 0)]}{1 - r_{\text{TM}}^{(g)}(\omega, 0)r_{\text{TM}}^{(p)}(\omega, 0)}, \quad (1)$$

where $r_{\text{TM}}^{(g)}$ and $r_{\text{TM}}^{(p)}$ are the TM reflection coefficients on graphene and on a plate taken singly, respectively (see Appendix for more details). The magnitude of the wave vector projection on the plane of graphene is put equal to zero because we consider the normal incidence.

The TM reflection coefficient of the electromagnetic waves on a freestanding graphene sheet is expressed as [47, 71]

$$r_{\text{TM}}^{(g)}(\omega, 0) = \frac{\tilde{\Pi}_{00}(\omega, 0)}{2 + \tilde{\Pi}_{00}(\omega, 0)}, \quad (2)$$

where the 00 component of the normalized polarization tensor of graphene $\tilde{\Pi}_{00}(\omega, 0)$ is connected with the conventional definition of the 00 component of this tensor by [71]

$$\tilde{\Pi}_{00}(\omega, 0) = -\frac{i\omega}{\hbar c} \lim_{k \rightarrow 0} \frac{\Pi_{00}(\omega, k)}{k^2}. \quad (3)$$

The explicit expression for the quantity Π_{00} for graphene with nonzero Δ and μ at any temperature T is presented in [60] (see Appendix concerning different but equivalent expressions for the reflection coefficients on a freestanding graphene sheet in terms of the polarization tensor, electric susceptibility and density-density correlation functions).

For us it is now important that the 00 component of the polarization tensor is directly connected with the in-plane conductivity of graphene [45, 58–60]

$$\Pi_{00}(\omega, k) = \frac{4\pi i \hbar k^2}{\omega} \sigma(\omega, k). \quad (4)$$

Combining this equation with (3), one obtains

$$\tilde{\Pi}_{00}(\omega, 0) = \frac{4\pi}{c}\sigma(\omega, 0). \quad (5)$$

As a result, the TM reflection coefficient on graphene (2) is expressed in terms of the in-plane conductivity

$$r_{\text{TM}}^{(g)}(\omega, 0) = \frac{2\pi\sigma(\omega, 0)}{c + 2\pi\sigma(\omega, 0)}. \quad (6)$$

Now we return to the reflection coefficient $r_{\text{TM}}^{(p)}$ on an uncoated dielectric plate. At the normal incidence it is given by the commonly known expression

$$r_{\text{TM}}^{(p)}(\omega, 0) = \frac{\sqrt{\varepsilon(\omega) - 1}}{\sqrt{\varepsilon(\omega) + 1}} = \frac{n(\omega) - 1 + ik(\omega)}{n(\omega) + 1 + ik(\omega)}, \quad (7)$$

where $\varepsilon(\omega)$ is the frequency-dependent dielectric permittivity of the plate material and $n(\omega)$ and $k(\omega)$ are the real and imaginary parts of its complex index of refraction, respectively. Representing the complex conductivity of graphene as

$$\sigma(\omega, 0) = \text{Re}\sigma(\omega) + i\text{Im}\sigma(\omega, 0), \quad (8)$$

and substituting (6)–(8) in (1), one finds the reflection coefficient on a graphene-coated plate

$$r_{\text{TM}}^{(g,p)}(\omega, 0) = \frac{n(\omega) - 1 + \frac{4\pi}{c}\text{Re}\sigma(\omega, 0) + i[k(\omega) + \frac{4\pi}{c}\text{Im}\sigma(\omega, 0)]}{n(\omega) + 1 + \frac{4\pi}{c}\text{Re}\sigma(\omega, 0) + i[k(\omega) + \frac{4\pi}{c}\text{Im}\sigma(\omega, 0)]}. \quad (9)$$

From (9) one easily obtains the reflectance of the plate coated with a graphene sheet

$$\begin{aligned} \mathcal{R}(\omega) &= [r_{\text{TM}}^{(g,p)}(\omega, 0)]^2 \\ &= \frac{[n(\omega) - 1 + \frac{4\pi}{c}\text{Re}\sigma(\omega, 0)]^2 + [k(\omega) + \frac{4\pi}{c}\text{Im}\sigma(\omega, 0)]^2}{[n(\omega) + 1 + \frac{4\pi}{c}\text{Re}\sigma(\omega, 0)]^2 + [k(\omega) + \frac{4\pi}{c}\text{Im}\sigma(\omega, 0)]^2}. \end{aligned} \quad (10)$$

The exact expressions for real and imaginary parts of the in-plane conductivity of graphene $\sigma(\omega, 0)$ have been found in [60] by using the polarization tensor. For the real part it was obtained

$$\text{Re}\sigma(\omega, 0) = \sigma_0\theta(\hbar\omega - \Delta)\frac{(\hbar\omega)^2 + \Delta^2}{2(\hbar\omega)^2} \left(\tanh \frac{\hbar\omega + 2\mu}{4k_B T} + \tanh \frac{\hbar\omega - 2\mu}{4k_B T} \right), \quad (11)$$

where the universal conductivity of graphene is $\sigma_0 = e^2/(4\hbar)$, the step function takes the values $\theta(x) = 1$, $x \geq 0$ and $\theta(x) = 0$, $x < 0$, and k_B is the Boltzmann constant.

The imaginary part for the in-plane conductivity of graphene is somewhat more complicated [60]

$$\text{Im}\sigma(\omega, 0) = \frac{\sigma_0}{\pi} \left[\frac{2\Delta}{\hbar\omega} - \frac{(\hbar\omega)^2 + \Delta^2}{(\hbar\omega)^2} \ln \left| \frac{\hbar\omega + \Delta}{\hbar\omega - \Delta} \right| + Y(\omega, \Delta, \mu) \right], \quad (12)$$

where the quantity Y is defined as

$$\begin{aligned} Y(\omega, \Delta, \mu) &= 2 \int_{\Delta/(\hbar\omega)}^{\infty} dt \sum_{\kappa=\pm 1} \left(\exp \frac{\hbar\omega t + 2\kappa\mu}{2k_B T} + 1 \right)^{-1} \\ &\times \left[1 + \frac{(\hbar\omega)^2 + \Delta^2}{(\hbar\omega)^2} \frac{1}{t^2 - 1} \right]. \end{aligned} \quad (13)$$

Note that equations (11)–(13) are exact in the framework of the Dirac model. They are derived on the basis of first principles of quantum electrodynamics at nonzero temperature. Taking into account that the Dirac model is applicable at sufficiently low frequencies ($\hbar\omega < 1 - 2$ eV), one arrives at the conclusion that these equations give the proper description of all physical properties dealing with electrical conductivity and reflection of light from graphene in this frequency region. We remind that the imaginary part of the dielectric permittivity of graphene, which is proportional to the real part (11) of its conductivity, is nonzero over the wide frequency region. This means that the concept of free Dirac quasiparticles allows the proper account of energy losses by conduction electrons in graphene due to scattering processes without resort to any additional parameters like in the 2-dimensional Drude model [14] or Kubo approach [74].

Although physics behind (11)–(13) was already discussed in the literature [60], we briefly recall the meaning of different contributions to the conductivity. Thus, the real part of conductivity (11) is interpreted as originating from the interband transitions [60,75]. The imaginary part of conductivity (12) contains contributions from both the interband and intraband transitions. To separate them analytically, one needs, however, to consider several distinct asymptotic regions of parameters in the quantity Y defined in (13), as is done in detail in [60]. For one example, under the conditions $k_B T \ll \mu$, $\hbar\omega \ll 2\mu$, and $\Delta < 2\mu$ one arrives at [60]

$$\text{Im}\sigma(\omega, 0) = \frac{\sigma_0}{\pi} \left[\frac{4\mu}{\hbar\omega} - 4 \ln 2 \frac{k_B T}{\hbar\omega} - \frac{(\hbar\omega)^2 + \Delta^2}{(\hbar\omega)^2} \ln \frac{2\mu + \hbar\omega}{2\mu - \hbar\omega} \right]. \quad (14)$$

Here, the first two terms on the right-hand side correspond to the intraband transitions, whereas the third term originates from the interband transitions [7,60] (see Ref. [60] for other relationships between $\hbar\omega$, T , μ , and Δ in (12) and (13)).

Using (10)–(13) and the optical data for the complex index of refraction of the plate material (see, for instance, [76]), one can calculate the reflectance of any material plate coated with real graphene sheet possessing nonzero energy gap and chemical potential. Such computations are presented in the next sections.

3. Reflectance as the function of frequency and chemical potential at a varying energy gap

We apply the formalism of Sec. II to describe the reflectance of a fused silica (SiO_2) plate coated with a graphene sheet. It has been known that fused silica plates are of frequent use as graphene substrates [77–81]. This material is characterized by the static dielectric permittivity $\varepsilon(0) \approx 3.82$ which remains unchanged up to rather high frequency $\hbar\omega = 10$ meV [76]. At higher frequencies the detailed optical data for $n(\omega)$ and $k(\omega)$ for SiO_2 are contained in [76].

Numerical computations of the reflectance of graphene-coated SiO_2 plate are performed by using (10)–(13). We start with the dependence of reflectance on frequency for three different values of the chemical potential and varying energy gap. The computational results are shown in figures 1(a), 1(b) and 1(c) at three temperatures

$T = 300$ K, 77 K, 4.4 K, respectively. In each of the the gray regions from left to right are plotted for the values of the chemical potential $\mu = 0, 0.1, \text{ and } 0.8$ eV, respectively. The width of the gray regions is caused by the values of the energy gap which varies from $\Delta = 0.1$ eV (the left boundary line of each region) to $\Delta = 0$ (the right boundary line of each region). The bottom lines in 1(a), 1(b) and 1(c), which are horizontal at $\hbar\omega \leq 10$ meV, demonstrate the reflectance of an uncoated SiO_2 plate. It is obtained from (10) by putting $\sigma(\omega, 0) = 0$

$$\mathcal{R}_0(\omega) = \frac{[n(\omega) - 1]^2 + k^2(\omega)}{[n(\omega) + 1]^2 + k^2(\omega)}. \quad (15)$$

In the frequency region $\hbar\omega \leq 10$ meV we have $k(\omega) = 0$ [76] and (15) reduces to

$$\mathcal{R}_0(\omega) = \left[\frac{\sqrt{\varepsilon(0)} - 1}{\sqrt{\varepsilon(0)} + 1} \right]^2 \approx 0.1044. \quad (16)$$

As is seen in figure 1, at the very low frequencies the reflectance of a graphene-coated SiO_2 plate is close to unity and drops to the reflectance of an uncoated plate with increasing frequency. Physically this means that at low frequencies the graphene coating behaves like a metallic one, whereas at high frequencies becomes transparent. The frequency region, where this drop takes place, shifts to higher frequencies with increasing chemical potential of graphene. The width of the gray regions (i.e., the range of frequencies where the energy gap of graphene sheet varies between zero and 0.1 eV) quickly decreases with increasing μ . This means that for larger μ an impact of the energy gap on the reflectance quickly decreases and for $\mu = 0.8$ eV there is no impact of Δ on the reflectance at any temperature. With decreasing temperature, some of the gray regions become wider. This feature is especially pronounced for the undoped graphene ($\mu = 0$). Thus, at $T = 77$ K and 4.4 K the left boundaries of the left gray regions are missing because they appear at much lower frequencies than those ones shown in figures 1(b) and 1(c). Note that for any reflectance smaller than unity the widths of all gray regions increase with decreasing frequency, but decrease when the reflectance approaches unity. The right boundary lines of the left gray regions in figures 1(a) and 1(b), plotted for the case $\mu = \Delta = 0$ at $T = 300$ K and 77 K, coincide with the lines 3 and 2, respectively, obtained earlier for this particular case in [68].

It is interesting that at a fixed frequency the increase of μ typically leads to a larger (or the same) reflectance, whereas the increase of Δ results in a smaller (or the same) reflectance, i.e., both quantities act in opposite directions. This effect has simple physical explanation. Thus, increasing μ leads to an increased density of charge carriers and increased conductivity resulting in the higher reflectance. Just to the opposite, an increased energy gap leads to the decreased mobility of charge carriers, decreased conductivity and, finally, to the lower reflectance. At $\hbar\omega \geq 20$ meV the graphene coating does not make any impact on the reflectance. Note that here and below we do not show the unobservable infinitesimally narrow peaks $\mathcal{R} = 1$ which appear under the condition $\hbar\omega = \Delta$ (see [70] for a discussion of this artefact).

Now we consider a dependence of the reflectance on the chemical potential. This is done separately at three different temperatures. In figure 2, the reflectance of a graphene-coated plate is shown as a function of μ at $T = 300$ K. The four gray regions from top to bottom are plotted for the frequency $\hbar\omega = 0.1, 1, 5,$ and 10 meV, respectively. In each of these regions, the upper boundary line is plotted for the energy gap $\Delta = 0$ and the lower boundary line for $\Delta = 0.1$ eV. The dashed lines are computed for $\Delta = 0.05$ eV. They are depicted only for sufficiently wide gray regions related to $\hbar\omega = 0.1$ and 1 meV. As is seen in figure 2, with increasing μ an impact of the energy gap on the reflectance quickly decreases in line with figure 1. The reflectance is the monotonously increasing function of μ . The maximum values of reflectance are reached faster for the light of lower frequency.

Next, we present the computational results for the reflectance as a function of μ at $T = 77$ K. In figure 3 it is plotted (a) at $\hbar\omega = 0.1$ meV and (b) at $\hbar\omega = 1.0$ meV. The upper and lower boundary lines of the gray regions are plotted for the energy gap $\Delta = 0$ and 0.1 eV, respectively, whereas the dashed middle lines for $\Delta = 0.05$ eV. In an inset to figure 3(b) the region of small values of $\mu \leq 0.12$ eV is shown on an enlarged scale. As can be seen in figure 3, the reflectance is again a monotonously increasing function of μ . At $\omega = 1.0$ meV [see figure 3(b)] the lower boundary line of the dashed region ($\Delta = 0.1$ eV) is very similar to the respective line in figure 2 plotted at $T = 300$ K and differs from it by only a more sharp angle. From figure 3(a) it is seen that for $\mu \geq 0.12$ eV the reflectance $\mathcal{R} = 1$ and does not depend on μ . At $\hbar\omega = 1.0$ meV the reflectance approaches to unity at much larger $\mu \approx 0.8$ eV [see figure 3(b)]. We do not present the computational results for a reflectance at $\hbar\omega = 5$ and 10 meV because at $T = 77$ K they are nearly the same as at $T = 300$ K (see figure 2).

Finally, we repeat computations of the reflectance of a graphene-coated SiO_2 plate as a function of μ at $T = 4.4$ K. The computational results are shown in figures 4(a) and 4(b) for the values of frequency $\hbar\omega = 0.1$ and 1.0 meV, respectively. All notations are the same as already explained in figures 3(a) and 3(b). It is seen that figure 4(a) differs from figure 3(a) plotted at $\omega = 0.1$ meV, $T = 77$ K by a sharper angle of the lower line restricting the gray region. It is seen also that at $\hbar\omega = 0.1$ meV, $T = 4.4$ K the graphene coating with $\mu = 0$ does not influence on the reflectance at any value of the energy gap from 0 to 0.1 eV (this is not the case at $\hbar\omega = 0.1$ meV, $T = 77$ K). Figure 4(b) plotted at $\hbar\omega = 1.0$ meV, $T = 4.4$ K differs from figure 3(b) plotted at the same frequency but $T = 77$ K by only a sharper angle of the lower line restricting the gray region (see the inset). In this case at $\mu = 0$ the graphene coating does not make an impact on the reflectance at both 77 K and 4.4 K. At $T = 4.4$ K the computational results for the reflectance at the frequencies $\hbar\omega = 5$ and 10 meV, are again nearly the same as at $T = 300$ K. They are shown by the bottom line and by the next to it gray region in figure 2.

4. Reflectance as the function of energy gap under different chemical potentials and frequencies

In this section we present the computational results for the reflectance of a graphene-coated SiO₂ plate as a function of the energy gap. In so doing, the chemical potential μ may at times be fixed, whereas the frequency takes several values, and at other times the fixed quantity is the frequency and the chemical potential takes different values. All computations are again performed by using (10)–(13). In figure 5 the reflectance is shown as a function of Δ for graphene coating with $\mu = 0.01$ eV at (a) $T = 300$ K and (b) $T = 77$ K. In figure 5(a) the seven lines from top to bottom are plotted for the values of $\hbar\omega = 0.01, 0.05, 0.1, 0.25, 0.5, 1,$ and ≥ 5 meV, respectively. In figure 5(b) there are five lines for the values of $\hbar\omega = 0.01, 0.05, 0.1, 0.5$ and ≥ 1 eV. In both figures 5a and 5b the computational results do not change when $\hbar\omega$ becomes larger than 5 and 1 meV, respectively. When decreasing temperature to below 77 K, the computational results do not change, so that figure 5(b) remains applicable. As is seen in figure 5, the reflectance decreases monotonously with increasing Δ . At lower temperature this decrease goes on faster.

In figure 6 similar computational results for the reflectance as a function of Δ at $T = 300$ K for graphene coating with $\mu = 0.1$ eV. It is interesting that for the relatively large μ the reflectance is already temperature-independent, when decreasing T to below 300 K. Because of this, the computational results at $T = 77$ K and 4.4 K are not shown. The seven lines from top to bottom are plotted for $\hbar\omega = 0.01, 0.1, 0.5, 1, 2.5, 5,$ and 10 meV, respectively. As is seen in figure 6, in this case the reflectance varies with μ very slowly.

Now we consider the dependence of the reflectance on energy gap at the fixed frequency and different values of μ . In figure 7 the reflectance of a graphene-coated plate is shown as a function of the energy gap at $\hbar\omega = 0.1$ meV and (a) $T = 300$ K, (b) $T = 77$ K, and (c) $T = 4.4$ K. The seven lines from bottom to top are plotted for the values of chemical potential $\mu = 0, 0.01, 0.03, 0.05, 0.07, 0.1,$ and ≥ 0.5 eV, respectively. As is seen in figure 7, the reflectance is again a decreasing function of Δ . At fixed Δ it takes either larger or the same values for larger chemical potential. With decreasing temperature, a decrease of the reflectance with increasing Δ becomes faster. At $T = 4.4$ K [figure 7(c)] the graphene coating with $\mu = 0$ does not influence on the reflectance shown by the bottom line. At fixed Δ the impact of temperature on the reflectance is more pronounced for graphene coating with smaller chemical potential. This is because at zero temperature the properties of graphene with small μ are almost the same as for an undoped graphene.

Finally, in figure 8 the computational results for the reflectance are shown as the function of Δ at $\hbar\omega = 1$ meV and (a) $T = 300$ K, (b) $T = 77$ K (the values of the reflectance computed at $T = 77$ K do not change with further decreasing temperature). The seven lines from bottom to top are plotted for $\mu \leq 0.01$ eV, $\mu = 0.03, 0.07, 0.1, 0.2, 0.5,$ and 0.8 eV, respectively. As can be seen in figure 8, the top two lines corresponding

to the largest values of the chemical potential are nearly flat, i.e., the reflectance does not depend on Δ at any temperature $T \leq 300$ K. It is seen also that the respective lines in figures 8(a) and 8(b) are very similar, i.e., the impact of temperature is very minor for all considered values of the chemical potential.

5. Conclusions and discussion

In this paper, we have presented the formalism, based of the first principles of quantum electrodynamics at nonzero temperature, which allows to compute the reflectance of a dielectric plate coated with real graphene sheet possessing nonzero energy gap and chemical potential. In doing so, the graphene sheet is described by the polarization tensor in (2+1)-dimensional space-time, and the dielectric plate by the measured optical data for the complex index of refraction of the plate material. This formalism was applied to the case of a graphene-coated plate made of silica glass at room, liquid-nitrogen, and liquid-helium temperatures.

The results of numerical computations show that there is a nontrivial interplay in the joint action of the energy gap, chemical potential, frequency of the incident light, and temperature on the reflectance. According to our results, an increase of the chemical potential and the energy gap of graphene coating influences the reflectance in opposite directions by making it larger and smaller, respectively. The physical explanation for this result is provided. It is shown that at sufficiently low frequencies the reflectance of a graphene-coated plate approaches unity, but goes down to the reflectance of an uncoated plate at sufficiently high frequencies. In this respect graphene coating is qualitatively similar to a metallic film. At $\hbar\omega \geq 20$ meV the graphene coating does not affect the reflectance of a plate made of silica glass independently of the values of the energy gap and chemical potential. Temperature makes major impact on the reflectance for graphene coatings with relatively small chemical potential. For sufficiently high chemical potential, a decrease from the room temperature down to the liquid-helium value does not influence on the reflectance.

We underline that the graphene coating significantly affects the reflectance only at frequencies below approximately $\hbar\omega = 20$ meV, i.e., fully in the application region of the Dirac model which extends up to 1–2 eV. This means that the developed formalism can be reliably used for controlling the reflectance of graphene-coated plates, e.g., for making it larger or smaller, by modifying the frequency, temperature, energy gap or the doping concentration.

It would be of much interest to compare the predicted effects with experimental data. Currently, however, available experiments are performed at higher frequencies. Thus, the reflectance of graphene-coated SiO₂ substrates was measured at $\hbar\omega$ above 60 meV [84], 130 meV [85], and 500 meV [75]. In these frequency regions, an impact of graphene on the reflectance of a substrate is rather small and was found in agreement with calculations using the polarization tensor with $\Delta = \mu = 0$ [68, 69] (note that with increasing frequency the influence of nonzero Δ and μ on the graphene reflectance

decreases). The relative infrared reflectance of graphene deposited on a SiC substrate, investigated for different values of μ at $\hbar\omega \geq 12$ meV [86], is in qualitative agreement with the computational results presented in Fig. 1. We conclude that large impact of graphene coating on a substrate reflectance in the far infrared region and the possibilities to control it predicted above might be beneficial for numerous applications of graphene-coated plates mentioned in section 1.

Acknowledgments

V. M. M. was partially funded by the Russian Foundation for Basic Research Grant No. 19-02-00453 A. The work of V. M. M. was also partially supported by the Russian Government Program of Competitive Growth of Kazan Federal University.

Appendix

In this Appendix, we derive the basic expression (1) for the reflection coefficient of a graphene-coated plate [46]. We also consider how the reflection coefficients of a graphene sheet are expressed via the polarization tensor of graphene and other related quantities such as the electric susceptibility and the density-density correlation function. This helps to understand equations (2)–(4).

Let us consider the system consisting of a graphene sheet, characterized by the amplitude reflection coefficient $r^{(g)}(\omega, k)$ and the transmission coefficient $t^{(g)}(\omega, k)$ spaced in vacuum at a height a above thick dielectric plate characterized by the amplitude reflection coefficient $r^{(p)}(\omega, k)$. These coefficients can be either transverse magnetic (TM) or transverse electric (TE). With account of multiple reflections on the graphene sheet and on the top boundary plane of the dielectric plate, the reflection coefficient of our system takes the form [82]

$$\begin{aligned} r^{(g,p)}(\omega, k) &= r^{(g)}(\omega, k) + t^{(g)}(\omega, k)r^{(p)}(\omega, k)t^{(g)}(\omega, k)e^{2iap(\omega,k)} \\ &\quad \times \sum_{n=0}^{\infty} \left[r^{(g)}(\omega, k)r^{(p)}(\omega, k)e^{2iap(\omega,k)} \right]^n \\ &= r^{(g)}(\omega, k) + \frac{t^{(g)}(\omega, k)r^{(p)}(\omega, k)t^{(g)}(\omega, k)e^{2iap(\omega,k)}}{1 - r^{(g)}(\omega, k)r^{(p)}(\omega, k)e^{2iap(\omega,k)}}, \end{aligned} \quad (\text{A.1})$$

where $p(\omega, k) = (\omega^2/c^2 - k^2)^{1/2}$.

Taking into account that for a graphene sheet in vacuum in the case of TM polarization of the electromagnetic field one has $t^{(g)}(\omega, k) = 1 - r^{(g)}(\omega, k)$ [83], (A.1) can be rewritten in the form

$$r_{a,\text{TM}}^{(g,p)}(\omega, k) = \frac{r_{\text{TM}}^{(g)}(\omega, k) + r_{\text{TM}}^{(p)}(\omega, k)[1 - 2r_{\text{TM}}^{(g)}(\omega, k)]e^{2iap(\omega,k)}}{1 - r_{\text{TM}}^{(g)}(\omega, k)r_{\text{TM}}^{(p)}(\omega, k)e^{2iap(\omega,k)}}, \quad (\text{A.2})$$

By considering the limiting case $a \rightarrow 0$ in (A.2), one obtains the reflection coefficient

[46]

$$r_{0,\text{TM}}^{(g,p)}(\omega, k) \equiv r_{\text{TM}}^{(g,p)}(\omega, k) = \frac{r_{\text{TM}}^{(g)}(\omega, k) + r_{\text{TM}}^{(p)}(\omega, k)[1 - 2r_{\text{TM}}^{(g)}(\omega, k)]}{1 - r_{\text{TM}}^{(g)}(\omega, k)r_{\text{TM}}^{(p)}(\omega, k)}, \quad (\text{A.3})$$

which coincides with (1) at the normal incidence $k = 0$.

The TM reflection coefficient of the electromagnetic waves on a graphene sheet can be written in the form [4, 6, 21]

$$r_{\text{TM}}^{(g)}(\omega, k) = \frac{p(\omega, k)\alpha(\omega, k)}{ik + p(\omega, k)\alpha(\omega, k)}, \quad (\text{A.4})$$

where the longitudinal (in-plane) electric susceptibility (polarizability) of graphene $\alpha(\omega, k)$ is expressed via the respective dielectric permittivity and density-density correlation function as

$$\alpha(\omega, k) = \varepsilon(\omega, k) - 1 = -\frac{2\pi e^2}{k}\chi(\omega, k). \quad (\text{A.5})$$

The latter is directly connected with the in-plane conductivity of graphene [21]

$$\sigma(\omega, k) = \frac{ie^2\omega}{k^2}\chi(\omega, k). \quad (\text{A.6})$$

Note that all the quantities α , ε , χ , and σ are also temperature-dependent.

The longitudinal (in-plane) density-density correlation function of graphene is expressed via the component Π_{00} of the polarization tensor [45]

$$\chi(\omega, k) = -\frac{1}{4\pi e^2\hbar}\Pi_{00}(\omega, k). \quad (\text{A.7})$$

In the framework of the Dirac model, the polarization tensor represents the effective action for massless (or very light) fermionic quasiparticles in the quadratic order of external electromagnetic field.

Substituting (A.5) and (A.7) in (A.4), one obtains the TM reflection coefficient on a graphene sheet in terms of the polarization tensor

$$r_{0,\text{TM}}^{(g)}(\omega, k) = \frac{p(\omega, k)\Pi_{00}(\omega, k)}{2i\hbar k^2 + p(\omega, k)\Pi_{00}(\omega, k)}, \quad (\text{A.8})$$

Introducing here the notation (3), one arrives at (2).

Then, by combining (A.6) with (A.7), we obtain equation (4).

References

- [1] Castro Neto A H, Guinea F, Peres N M R, Novoselov K S and Geim A K 2009 *Rev. Mod. Phys.* **81**, 109.
- [2] Katsnelson M I 2012 *Graphene: Carbon in Two Dimensions* (Cambridge: Cambridge University Press)
- [3] Aoki H and Dresselhaus M S (eds) 2014 *Physics of Graphene* (Cham: Springer)
- [4] Stauber T, Peres N M R and Geim A K 2008 *Phys. Rev. B* **78** 085432
- [5] Gusynin V P, Sharapov S G and Carbotte J P 2007 *Phys. Rev. Lett.* **98** 157402
- [6] Falkovsky L A and Pershoguba S S 2007 *Phys. Rev. B* **76** 153410
- [7] Falkovsky L A 2008 *J. Phys.: Conf. Ser.* **129** 012004

- [8] Pedersen T G, Jauho A-P and Pedersen K 2009 *Phys. Rev. B* **79** 113406
- [9] Merano M 2016 *Phys. Rev. A* **93** 013832
- [10] Auslender M and Katsnelson M I 2007 *Phys. Rev. B* **76** 235425
- [11] Scholz A and Schliemann J 2011 *Phys. Rev. B* **83** 235409
- [12] Dartora C A and Cabrera G G 2013 *Phys. Rev. B* **87** 165416
- [13] Liu D and Zhang S 2008 *J. Phys.: Condens. Matter* **20** 175222
- [14] Horng J *et al* 2011 *Phys. Rev. B* **83** 165113
- [15] Dobson J F, White A and Rubio A 2006 *Phys. Rev. Lett.* **96** 073201
- [16] Gómez-Santos G 2009 *Phys. Rev. B* **80** 245424
- [17] Drosdoff D and Woods L M 2010 *Phys. Rev. B* **82** 155459
- [18] Drosdoff D and L. M. Woods L M 2011 *Phys. Rev. A* **84** 062501
- [19] Bo E. Sernelius Bo E 2011 *Europhys. Lett.* **95** 57003
- [20] Judd T E, Scott R G, Martin A M, Kaczmarek B and Fromhold T M 2011 *New J. Phys.* **13** 083020
- [21] Sernelius Bo E 2012 *Phys. Rev. B* **85** 195427
- [22] Sarabadani J, Najji A, Asgari R and Rodgornik R 2011 *Phys. Rev. B* **84** 155407
- [23] Sarabadani J, Najji A, Asgari R and Rodgornik R 2013 *Phys. Rev. B* **87** 239905
- [24] Drosdoff D, Phan A D, Woods L M, Bondarev I V and Dobson J F 2012 *Eur. Phys. J. B* **85** 365
- [25] Tse W-K and MacDonald A H 2012 *Phys. Rev. Lett.* **109** 236806
- [26] Cysne T, Kort-Kamp W J M, Oliver D, Pinheiro F A, Rosa F S S and Farina C 2014 *Phys. Rev. A* **90** 052511
- [27] Svetovoy V B and Palasantzas G 2014 *Phys. Rev. Appl.* **2** 034006
- [28] Khusnutdinov N, Kashapov R and Woods L M 2016 *Phys. Rev. A* **94** 012513
- [29] Ziegler K 2006 *Phys. Rev. Lett.* **97** 266802
- [30] Lewkowicz M and B. Rosenstein B 2009 *Phys. Rev. Lett.* **102** 106802
- [31] Klimchitskaya G L and Mostepanenko V M 2013 *Phys. Rev. B* **87** 075439
- [32] Gorbar E V, Gusynin V P, Miransky V A and Shovkovy I A 2002 *Phys. Rev. B* **66** 045108
- [33] Gusynin V P and Sharapov S G 2006 *Phys. Rev. B* **73** 245411
- [34] Pyatkovsky P K 2009 *J. Phys.: Condens. Matter* **21** 025506
- [35] Bordag M, Fialkovsky I V, Gitman D M and Vassilevich D V 2009 *Phys. Rev. B* **80** 245406
- [36] Fialkovsky I V, Marachevsky V N and Vassilevich D V 2011 *Phys. Rev. B* **84** 035446
- [37] Bordag M, Klimchitskaya G L and Mostepanenko V M 2012 *Phys. Rev. B* **86** 165429
- [38] Chaichian M, Klimchitskaya G L, Mostepanenko V M and Tureanu A 2012 *Phys. Rev. A* **86** 012515
- [39] Arora B, Kaur H and B. K. Sahoo B K 2014 *J. Phys. B* **47** 155002
- [40] Kaur K, Kaur J, Arora B and Sahoo B K 2014 *Phys. Rev. B* **90** 245405
- [41] Klimchitskaya G L and Mostepanenko V M 2014 *Phys. Rev. A* **89** 012516
- [42] Klimchitskaya G L and Mostepanenko V M 2014 *Phys. Rev. B* **89** 035407
- [43] Klimchitskaya G L and Mostepanenko V M 2014 *Phys. Rev. A* **89** 052512
- [44] Klimchitskaya G L and Mostepanenko V M 2014 *Phys. Rev. A* **89** 062508
- [45] Klimchitskaya G L, Mostepanenko V M and Sernelius Bo E 2014 *Phys. Rev. B* **89** 125407
- [46] Klimchitskaya G L, Mohideen U and Mostepanenko V M 2014 *Phys. Rev. B* **89** 115419
- [47] Bordag M, Klimchitskaya G L, Mostepanenko V M and Petrov V M 2015 *Phys. Rev. D* **91** 045037
- [48] Bordag M, Klimchitskaya G L, Mostepanenko V M and Petrov V M 2016 *Phys. Rev. D* **93** 089907
- [49] Bordag M, Fialkovskiy I and Vassilevich D 2016 *Phys. Rev. B* **93** 075414
- [50] Bordag M, Fialkovskiy I and Vassilevich D 2017 *Phys. Rev. B* **95** 119905
- [51] Klimchitskaya G L and Mostepanenko V M 2015 *Phys. Rev. B* **91** 174501
- [52] Klimchitskaya G L 2016 *Int. J. Mod. Phys. A* **31** 1641026
- [53] Bezerra V B, Klimchitskaya G L, Mostepanenko V M and Romero C 2016 *Phys. Rev. A* **94** 042501
- [54] Bimonte G, Klimchitskaya G L and Mostepanenko V M 2017 *Phys. Rev. A* **96** 012517
- [55] Bimonte G, Klimchitskaya G L and Mostepanenko V M 2017 *Phys. Rev. B* **96** 115430
- [56] Henkel C, Klimchitskaya G L and Mostepanenko V M 2018 *Phys. Rev. A* **97** 032504
- [57] Klimchitskaya G L and Mostepanenko V M 2018 *Phys. Rev. A* **98** 032506

- [58] Klimchitskaya G L and Mostepanenko V M 2016 *Phys. Rev. B* **93** 245419
- [59] Klimchitskaya G L and Mostepanenko V M 2016 *Phys. Rev. B* **94** 195405
- [60] Klimchitskaya G L, Mostepanenko V M and Petrov V M 2017 *Phys. Rev. B* **96** 235432
- [61] Klimchitskaya G L and Mostepanenko V M 2018 *Phys. Rev. D* **97** 085001
- [62] Klimchitskaya G L and Mostepanenko V M 2016 *Phys. Rev. A* **93** 052106
- [63] Klimchitskaya G L, Mostepanenko V M and Petrov V M 2018 *Phys. Rev. A* **98** 023809
- [64] Bludov Yu V, Vasilevskiy M I and N. M. R. Peres N M R 2010 *Europhys. Lett.* **92** 68001
- [65] Chung K, Lee C-H and Yi G-C 2010 *Science* **330** 655
- [66] Hong W, Xu Y, Lu G, Li C and Shi G 2008 *Electrochem. Commun.* **10** 1555
- [67] Kuila T, Bose S, Khanra P, Mishra A K, Kim N H and Lee J H 2011 *Biosens. Bioelectron.* **29** 4637
- [68] Klimchitskaya G L, Korikov C C and Petrov V M 2015 *Phys. Rev. B* **92** 125419
- [69] Klimchitskaya G L, Korikov C C and Petrov V M 2016 *Phys. Rev. B* **93** 159906
- [70] Klimchitskaya G L and Mostepanenko V M 2017 *Phys. Rev. B* **95** 035425
- [71] Klimchitskaya G L and Mostepanenko V M 2018 *Phys. Rev. A* **97** 063817
- [72] Gusynin V P, Sharapov S G and Carbotte J P 2009 *New J. Phys.* **11** 095013
- [73] Jafari S A 2012 *J. Phys.: Condens. Matter* **24** 205802
- [74] Falkowsky L A and Varlamov A A 2007 *Eur. Phys. J. B* **56** 281
- [75] Mak K F, Sfeir M Y, Wu Y, Lui C H, Misewich J A and Heinz T F 2008 *Phys. Rev. Lett.* **101** 196405
- [76] Palik E D (ed) 1985 *Handbook of Optical Constants of Solids* (New York: Academic Press)
- [77] Banishev A A, Wen H, Xu J, Kawakami R K, Klimchitskaya G L, Mostepanenko V M and Mohideen U 2013 *Phys. Rev. B* **87** 205433
- [78] da Gunha Rodrigues G, Zelenovskiy P, Romanyuk K, Luchkin S, Kopelevich Ya and Kholkin A 2015 *Nat. Commun.* **6** 7572
- [79] Kang Y-J, Kang J and Chang K J 2008 *Phys. Rev. B* **78** 115404
- [80] Ishigami M, Chen J H, Cullen W G, Fuhrer M S and Williams E D 2007 *Nano. Lett.* **7** 1643
- [81] Nguyen T C, Otani M and Okada S 2011 *Phys. Rev. Lett.* **106** 106801
- [82] Chew W C 1999 *Waves and Fields in Inhomogeneous Media* (New York: Wiley-IEEE Press)
- [83] Stauber T, Peres N M R and Geim A K 2008 *Phys. Rev. B* **78** 085432
- [84] Goldflam M D, Ruiz I, Howell S W, Wendt J R, Sinclair M B, Peters D W and Beechem T E 2018 *Opt. Express* **26** 8532
- [85] Saigal N, Mukherjee A, Sugunakar V and Ghosh S 2014 *Rev. Sci. Instr.* **85** 073105
- [86] Santos C N, Joucken F, De Sousa Meneses D, Echegut P, Campos-Delgado J, Louette P, Raskin J-P and Haskens B 2016 *Sci. Reports* **6** 2430

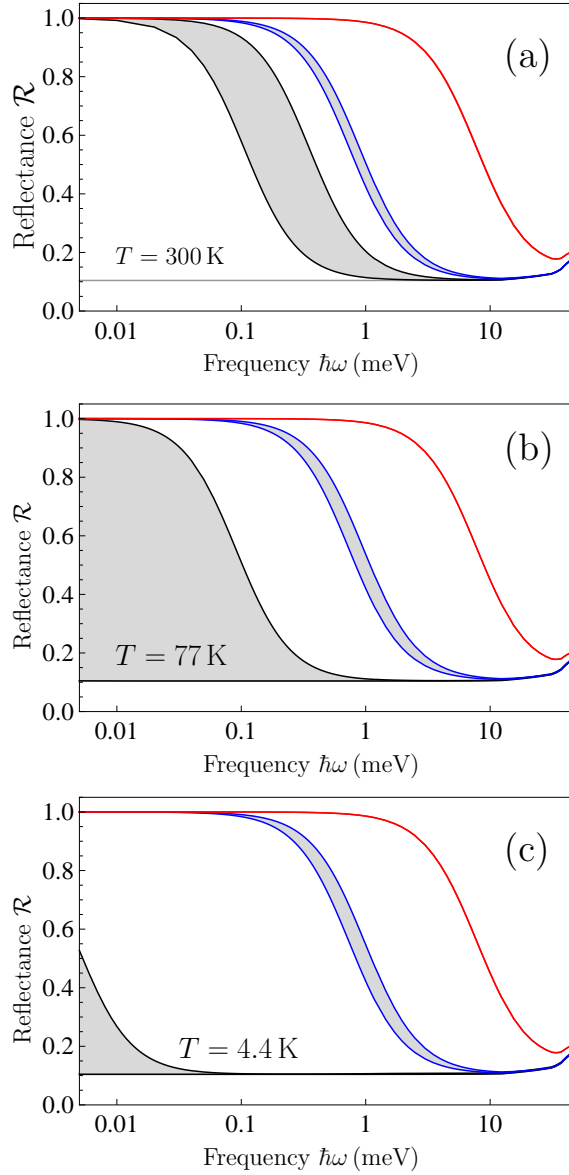


Figure 1. The reflectances of graphene-coated SiO_2 plate at the normal incidence are shown as functions of frequency at (a) $T = 300$ K, (b) $T = 77$ K, and (c) $T = 4.4$ K. The gray regions from left to right are plotted for the chemical potential $\mu = 0, 0.1,$ and 0.8 eV, respectively. The right and left boundary lines of each gray region are plotted for the energy gap $\Delta = 0$ and 0.1 eV, respectively.

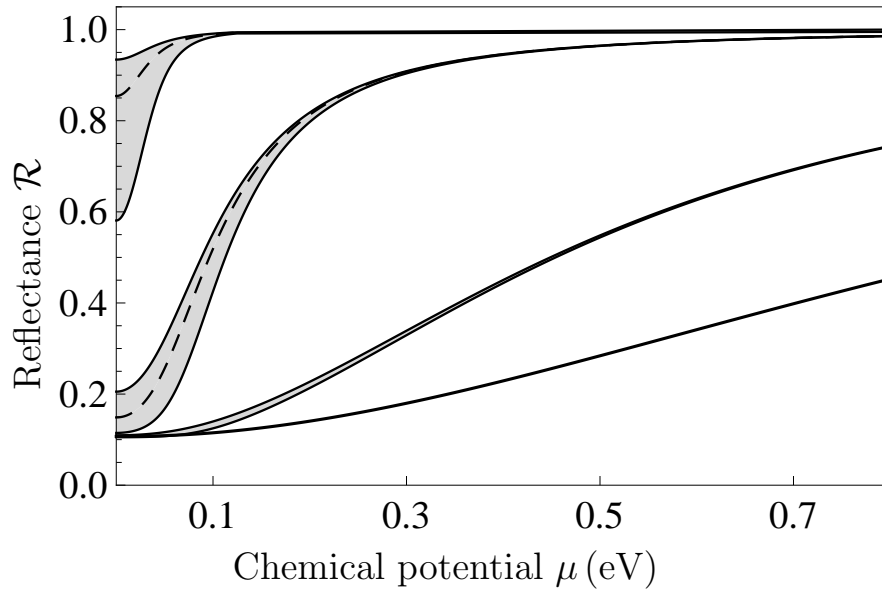


Figure 2. The reflectances of graphene-coated SiO_2 plate at the normal incidence are shown as functions of the chemical potential at $T = 300$ K. The gray regions from top to bottom are plotted for the frequency $\hbar\omega = 0.1, 1, 5,$ and 10 meV, respectively. The upper and lower boundary lines of each gray region are plotted for the energy gap $\Delta = 0$ and 0.1 eV, respectively, whereas the dashed middle lines are depicted for $\Delta = 0.05$ eV.

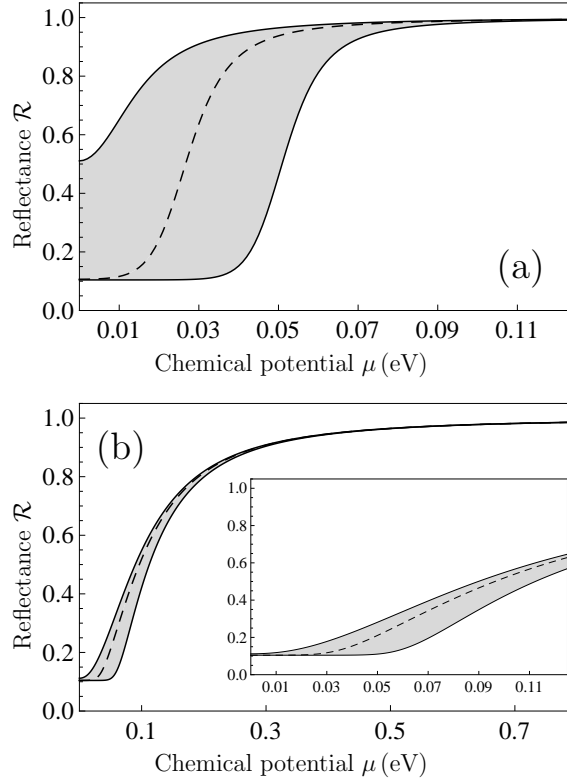


Figure 3. The reflectances of graphene-coated SiO_2 plate at the normal incidence are shown as functions of the chemical potential at $T = 77$ K and (a) $\hbar\omega = 0.1$ meV, (b) $\hbar\omega = 1.0$ meV. The upper and lower boundary lines of the gray regions are plotted for the energy gap $\Delta = 0$ and 0.1 eV, respectively, whereas the dashed middle lines for $\Delta = 0.05$ eV. The region of smaller μ is shown on an inset for $\hbar\omega = 1.0$ meV.

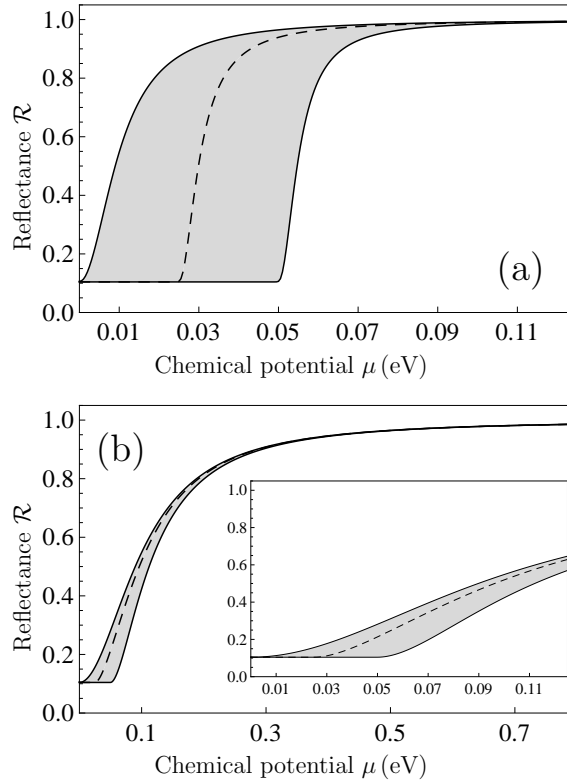


Figure 4. The reflectances of graphene-coated SiO_2 plate at the normal incidence are shown as functions of the chemical potential at $T = 4.4$ K and (a) $\hbar\omega = 0.1$ meV, (b) $\hbar\omega = 1.0$ meV. The upper and lower boundary lines of the gray regions are plotted for the energy gap $\Delta = 0$ and 0.1 eV, respectively, whereas the dashed middle lines for $\Delta = 0.05$ eV. The region of smaller μ is shown on an inset for $\hbar\omega = 1.0$ meV.

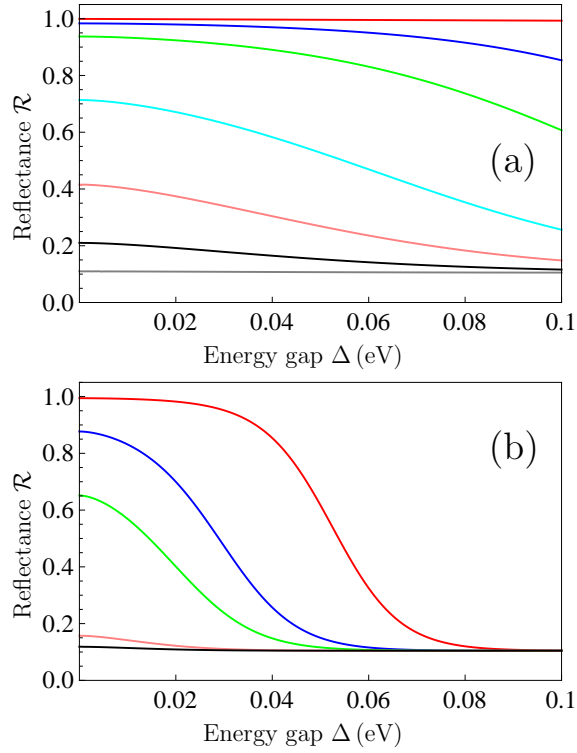


Figure 5. The reflectances of graphene-coated SiO_2 plate at the normal incidence are shown as functions of the energy gap for the chemical potential $\mu = 0.01$ eV and at (a) $T = 300$ K, (b) $T = 77$ K. The lines from top to bottom are plotted for (a) $\hbar\omega = 0.01, 0.05, 0.1, 0.25, 0.5, 1.0,$ and ≥ 5 meV, and (b) $\hbar\omega = 0.01, 0.05, 0.1, 0.5,$ and ≥ 1.0 meV, respectively.

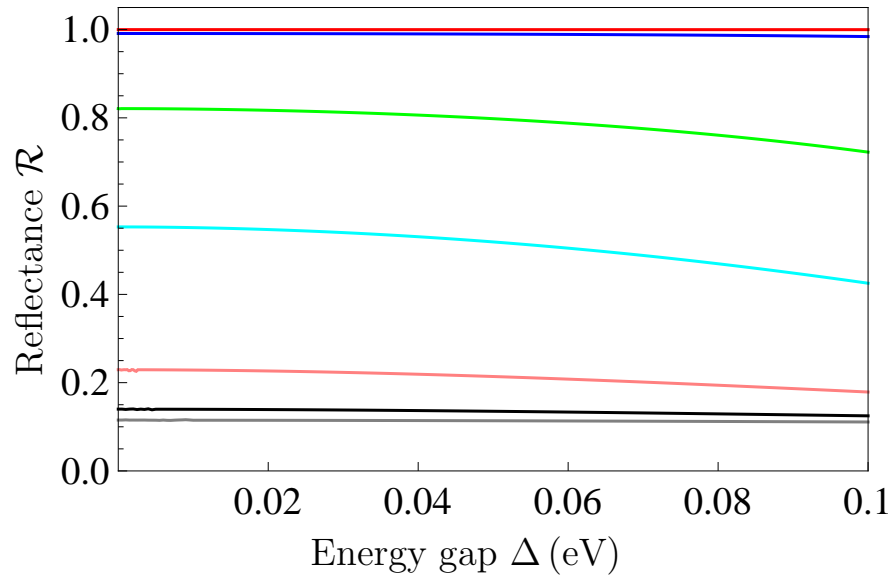


Figure 6. The reflectance of graphene-coated SiO₂ plate at the normal incidence is shown as a function of the energy gap for the chemical potential $\mu = 0.1$ eV at $T = 300$ K. The seven lines from top to bottom are plotted for $\hbar\omega = 0.01, 0.1, 0.5, 1.0, 2.5, 5,$ and 10 meV.

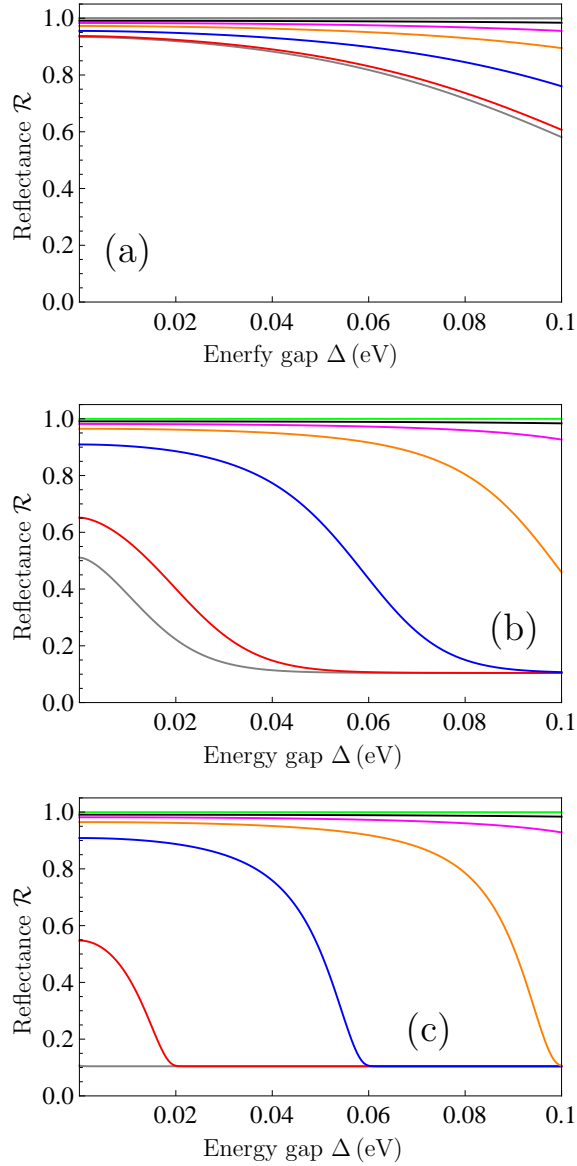


Figure 7. The reflectances of graphene-coated SiO_2 plate at the normal incidence are shown as functions of the energy gap for $\hbar\omega = 0.1$ eV at (a) $T = 300$ K, (b) $T = 77$ K, and (c) $T = 4.4$ K. The seven lines from bottom to top are plotted for the chemical potential $\mu = 0, 0.01, 0.03, 0.05, 0.07, 0.1,$ and ≥ 0.5 eV, respectively.

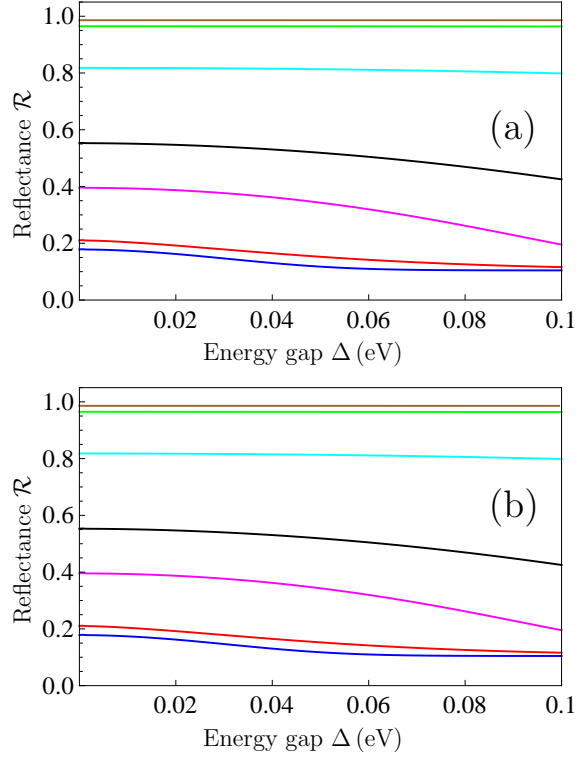


Figure 8. The reflectances of graphene-coated SiO_2 plate at the normal incidence are shown as functions of the energy gap for $\hbar\omega = 1$ meV at (a) $T = 300$ K and (b) $T = 77$ K. The seven lines from bottom to top are plotted for the chemical potential $\mu \leq 0.01$ eV, $\mu = 0.03$, 0.07 , 0.1 , 0.2 , 0.5 , and 0.8 eV, respectively.